Journal of Thermal Science Vol.31, No.3 (2022) 663–677

https://doi.org/10.1007/s11630-022-1596-7 **Article ID: 1003-2169(2022)03-0663-15**

Solar Flux Measuring and Optical Efficiency Forecasting of the Linear Fresnel Reflector Concentrator after Dust Accumulation

ZHAO Xiaoyan[1], YAN Suying[1*], ZHANG Na[2,3], ZHAO Ning[1], GAO Hongwei[1]

1. College of Energy and Power Engineering, Inner Mongolia University of Technology, Hohhot 010051, China
2. Institute of Engineering Thermophysics, Chinese Academy of Sciences, Beijing 100190, China
3. University of Chinese Academy of Sciences, Beijing 100049, China

Abstract: The linear Fresnel reflector concentrator (LFRC) is widely used in the field of solar energy utilization due to its simple structure, low cost, and excellent wind resistance. Nevertheless, the LFRC operates outdoors all year round, and the dust accumulation on the mirror will reduce the optical efficiency of the system, so it needs to be perfected and improved. In this paper, a focal plane energy flux experimental device was designed to test the energy flux of the system under different dust accumulation times. The results indicate that, the dust density on the mirror increased and the energy flux on the focal plane decreased with increase of dust accumulation time. After undergoing dust accumulation for 35 days, the dust density on the mirror reached 4.33 g/m^2 and the average energy flux on the focal plane decreased to 1.78 kW/m^2. Additionally, the variation of reflectivity caused by dust accumulation on mirror was taken as the quantitative index, and a prediction model for the impact of dust on the optical efficiency of the system was proposed. The results will provide guidance for improving the optical efficiency of the LFRC.

Keywords: dust accumulation, energy flux, linear Fresnel reflector concentrator, optical efficiency, forecast

1. Introduction

The progress and development of human science and technology depend on the speed of industrial development, which is closely related to energy consumption. Solar energy has the advantages of being clean, safe, environmentally friendly, and having large reserves, it has appropriately become one of the newer energy sources for humans to research and develop upon [1, 2]. The distribution of the solar spectrum was a kind of blackbody radiation at a temperature of 5778 K, which was close to the surface temperature of the Sun. Most of the solar radiation was concentrated in the infrared regions, visible regions, and ultraviolet regions [3–5]. The utilization of solar energy mainly includes photothermal conversion and photoelectric conversion. Due to the low solar radiation energy flux reaching the ground, a condensing device is needed to improve the solar radiation energy flux per unit area, such as the parabolic trough collector, linear Fresnel reflector concentrator (LFRC), solar tower, or solar dish [6–8]. Among them, the LFRC has been widely used in urban heating and solar power generation because of its low cost, small floor area, and simple structure [9]. As an outdoor application of solar concentrating and heat collecting, the LFRC is easily affected by solar irradiance,

Received: Dec 21, 2021 Corresponding author: YAN Suying E-mail: yansy@imut.edu.cn

Nomenclature

CCD	charge-coupled device	u_1	uncertainty component caused by the repeatability of measurement
CPC	compound parabolic collector	u_2	uncertainty component caused by the test accuracy of heat flux sensor
CSP	concentrating solar power	u_3	uncertainty component caused by the accuracy of the CCD camera
E	energy flux/kW·m^{-2}	u_4	uncertainty component caused by the error of Lambert target
E_{ave}	average energy flux on the light spot/kW·m^{-2}	**Greek symbols**	
E_{max}	maximum energy flux on the light spot/kW·m^{-2}	α	metal tube absorptivity of collector
ΔE	uniformity of light spot	γ	intercept factor
e_1	energy obtained by the receiver before dust accumulation/W	δ	dust accumulation density of the mirror
e_2	energy obtained by the receiver after the accumulation/W	η_0	optical efficiency
F_c	scale coefficient	η_{cpc}	geometric optical efficiency of CPC
$f(e)$	end loss coefficient of concentrator	θ	incidence angle/(°)
$f(i)$	shadow and occlusion loss coefficient of concentrator	κ	diaphaneity of dust
$f(\zeta)$	correction coefficient of the intercept factor	ζ	cleanliness Factor
G_b	direct solar radiation that actually incidents on the concentrator/W·m^{-2}	ρ	reflectivity of the plane mirror
G_D	direct solar radiation measured by the instrument/W·m^{-2}	ρ_0	theoretical reflectivity
LFRC	linear Fresnel reflector concentrator	ρ_1	reflectivity of the mirror before dust accumulation
PV	photovoltaic module	ρ_2	reflectivity of the mirror after dust accumulation
R	radius of dust/cm	τ	glass tube transmittance of collector
u_c	relative standard uncertainty of the energy flux	υ	density of the dust particles/g·cm^{-3}

weather, and operation conditions [10, 11]. In addition, during practical utilization, the dust accumulation on the surface of the solar reflector is inevitable, while its optical efficiency deteriorates and the solar collection performance declines [11]. Studying the dust accumulation law of mirrors can provide a basis of data for mirror dust removal, which is of great significance for improving the efficiency of solar reflectors.

The solar concentrator is generally operated outdoors all year round. The dust accumulation on the reflector reduces the reflectivity of the solar concentrator, resulting in optical loss and the eventual reduction in system efficiency [13–15]. Merrouni et al. [16] analyzed the influence of dust on the condenser reflectance of a photothermal power station in an arid area. According to a 12-week outdoor test in Eastern Morocco, it was found that the reflectance of the condenser decreased by 30% due to the accumulation of dust. Gholami et al. [17] studied the impact of dust accumulation on the solar PV module, the results showed that the transmittance decreased by 25% after the 70-day dust accumulation. Bellmann et al. [18] conducted the dust accumulation test on the main optical characteristics of the CSP condenser mirror and PV module. It was found that the optical pollution loss of CSP was 8–14 times higher than that of the PV module under the same dust accumulation density. Wu et al. [19] determined that the dust accumulated on the solar trough concentrator reduced the reflectivity by absorbing and scattering sunlight. When the reflectivity was less than 90%, the concentrator needed to be cleaned. Heimsath et al. [20] studied the influence of an incident angle on the accumulation of dust on the mirror, finding that the mirror reflectivity decreased significantly with the increase in incident angle. To provide a complete physical model to predict and evaluate the performance of the solar concentrator, Zhao et al. [21] comprehensively analyzed the mechanical behavior of dust particles in the process of movement and collision on the surface of the PV module. The effects of wind speed, humidity, and particle size on the characteristics of dust accumulation were simulated. The simulation results were compared with the test results to verify the rationality of the particle accumulation criterion and simulation method.

The above studies investigated the impact of dust accumulation on mirror reflectivity. When the concentrator reflectivity decreased because of the mirror dust, the most direct impact on the solar concentrating and heat collecting system was the decline in the energy flux on the focal plane. Therefore, it was necessary to test the decrease in the energy flux caused by the accumulation of dust.

The energy flux and the light spot uniformity on the focal plane play a key role in evaluating the focusing performance of the system [22]. Ballestrin et al. [23] introduced a method to directly measure the energy flux on the focusing plane utilizing a heat flow meter. Its main advantage is that the measurement uncertainty was low and water cooling was not required. A disadvantage of this method is that the installation number of the heat flow meters would directly affect the test accuracy. The indirect measurement method would use the CCD camera to capture the light spot image, and light scattering technology would be implemented to estimate the energy flux, which had higher spatial resolution [24]. Roldán et al. [25] used a high-resolution CCD device to capture the energy flux on the Lambert target, obtained the fitting function by evaluating the image descriptor value under normalization computing, and used the function to predict the energy flux distribution in any plane and under different operating conditions. Xiao et al. [26] experimentally studied the energy flux on the focal plane by implementing a Lambert target and CCD camera. Moreover, a calibration method based on spectral normalization calculation was proposed to reduce the spectral error. Until now, previous researchers have predominantly used the heat flux sensor, camera, and Lambert target to carry out relative tests on the energy flux to verify its reliability [27–28].

The main purpose of studying the optical performance decline caused by dust accumulation is to provide guidance for the optimal dust removal strategy. Predicting the impact of dust accumulation on optical performance and system efficiency can play an important role in exploring the best dust removal method and frequency. Previous studies have established an effective prediction model for the decline of transmittance caused by dust accumulation to evaluate the optimal cleaning time of the PV module [29–31]. Li and Sangchul [32, 33] proposed a comprehensive physical model based on the Lambert-Beer law to predict the effect of dust on the transmittance of solar panels. Picotti [34] used a physical model to evaluate the reduction of optical efficiency for each part of the concentrator and verified it by the practical case. Bouaddi [35] established a dynamic linear Gaussian state space-time series model to describe and predict the reflection loss of the concentrator in a CSP power plant. Heimsath [36] studied the dust accumulation of a mirror exposed to the desert and proposed a model to predict the mirror reflectivity with different levels of cleanliness. The model correlated the dust attenuation to the solar radiation with the incident angle, which was then applied to the prediction of the annual luminous efficiency of a parabolic trough power plant.

To summarize, relevant studies have focused on the impact of dust accumulation on the solar condensing mirror and the PV module. Additionally, most of these studies focus on the reduction of reflectivity or transmittance by dust accumulation. In fact, the most direct manifestation of the impact of dust accumulation on the performance of the solar concentrating and heat collecting system is the decline in the energy flux on the focal plane, but there are few reports on this topic at present. Studying the influence of dust on the energy flux of the focal plane can predict the influence of dust on the optical efficiency of the system, which is of great significance in determining the economy and effectiveness of a dust cleaning scheme.

In this paper, an energy flux experimental device based on a Lambert target, CCD camera, and heat flow meter was designed. The solar flux distribution on the focal plane of the LFRC under different dust accumulation times was measured. The main contributions of this study include the following: (1) the correlation of energy obtained on the focal plane of the LFRC under different dust densities was revealed; (2) the cleanliness factor of mirror was taken as the index to quantify the dust accumulation, and a prediction model was proposed for the impact of dust accumulation on the optical efficiency of the system; and (3) suggestions were proposed for the dust removal frequency in different seasons.

In the following contents, Section 2 introduces the influence mechanism of mirror dust on the LFRC. Section 3 describes the experimental system and method. The effects of the dust density on energy flux, light spot uniformity, and the intercept factor are presented in Section 4, and a prediction model for the effect of mirror dust on the optical efficiency of the system is proposed. Finally, the main conclusions are summarized in Section 5.

2. Dust Accumulation Mechanism and Quantification Method of the LFRC

2.1 Dust accumulation mechanism

The solar concentrating and heat collecting system generally operates outdoors all year round, and the floating dust in the atmosphere will settle on the surface of the mirror under the action of wind, especially in an area with frequent dust storms. The sources of dust

accumulation are mainly the sand and soil in the desert, pollutants discharged by factories, and vehicle exhaust. The dust settles on the ground and the solar concentrating mirror due to the interaction of gravity and high-altitude wind transportation.

Dust particles have non-transparent properties. The solar radiant energy incident on dust particles can be divided into three parts: the transmitted radiant energy, the radiant energy absorbed by dust, and the radiant energy reflected by dust. As shown in Fig. 1(a), the lights with intensity E has the energy of $\Delta E1$ can be transmitted, the energy of $\Delta E2$ can be scattered and the energy of $\Delta E3$ absorbed by dust. The transmitted lights are refracted in the dust particles. From the Lambert-Beer law, the intensity of light propagating through a medium can be expressed as follows [37]:

$$\frac{I}{I_0} = \mathrm{e}^{-A_\lambda} \tag{1}$$

where I_0 and I are the incident light intensity and the transmitted intensity, respectively. A_λ is the optical thickness, which is given by the following equation:

$$A_\lambda = Q_\mathrm{e} L = \alpha L \tag{2}$$

where Q_e is the attenuation coefficient of incident radiation through a particle, while L is the transmittance distance of light. L is related to the thickness, geometry, and refractive index of the medium. Some of the scattered lights can reach the receiver or be lost to the environment, and some may even reach the mirror again. As shown in Fig. 1(b), a part of the incident lights shine onto the mirror, follow the reflection law, and gather on the surface of the heat collecting tube along the direction of the reflected lights. Moreover, the other parts of the lights shine onto the dust particle, resulting in the reflection and the absorption deviating from the original path. Due to the difference between the size, shape, and transparency of the dust particles, the reflected lights cannot all gather on the collector tube, resulting in energy loss and ultimately reducing the optical efficiency of the LFRC.

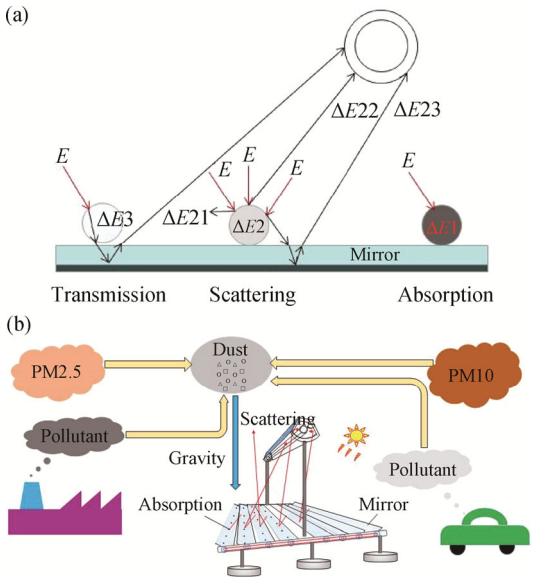

Fig. 1 The effect of dust accumulation on optical loss

2.2 Evaluation index

As for the solar concentrating system, the solar radiation reflected by the mirror cannot be projected onto the receiver. The amount of energy obtained from the receiver can be expressed by the intercept factor, which is defined as the percentage of solar radiation reflected by the mirror captured by the receiver, which is expressed as:

$$\gamma = \frac{\int_A^B I(W)\,\mathrm{d}W}{\int_{-\infty}^{\infty} I(W)\,\mathrm{d}W} \tag{3}$$

where W is the linear distance from the center line of the receiver to the edge, mm; and I is the energy flux, kW/m^2.

The dust on the mirror will reduce the reflectivity of the condenser mirror, which can affect energy collection on the focal plane. To better evaluate the impact, the concepts of "mirror cleanliness factor" and "correction coefficient of intercept factor" are introduced.

The cleanliness factor of mirror is defined as the ratio of mirror reflectivity after dust accumulation to that after cleaning [38].

$$\zeta = \frac{\rho_2}{\rho_1} = \rho_0 \exp\left[\frac{-3(1-\kappa)\delta}{4\nu}\int_R \frac{3}{16R^2}\,\mathrm{d}R\right] \tag{4}$$

where ζ is the cleanliness factor of the mirror; ρ_1 and ρ_2 denote the reflectance before and after dust accumulation, respectively; ρ_0 is the theoretical reflectance of the mirror; R is the radius of the dust (cm); κ is the dust transparency; υ is the density of dust particle (g/cm^3), and δ is the dust accumulation density of the mirror (g/m^2).

The correction coefficient of intercept factor is defined as the ratio of the focal plane energy corresponding to the dust deposition mirror to that corresponding to the clean mirror under the same operating conditions of the system.

$$f(\zeta) = e_2 / e_1 \tag{5}$$

where $f(\zeta)$ represents the correction factor of the intercept factor; while e_1 and e_2 represent the energy obtained by the receiver before and after dust accumulation, respectively.

3. Experimentation

3.1 Energy flux experiment device

As for the LFRC, the measurement devices of energy flux based on the combination of the CCD camera and heat flux sensor are designed. As shown in Fig. 2, the

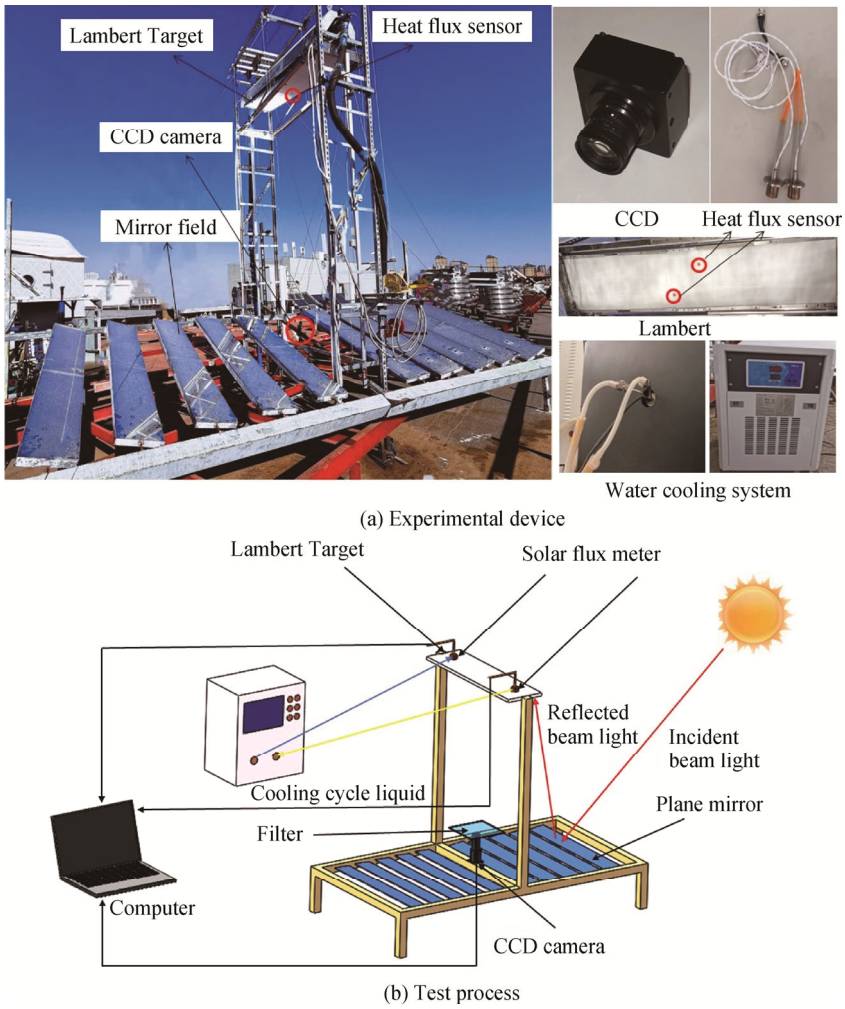

Fig. 2 Linear Fresnel system energy flux measurement system

system is mainly composed of a CCD industrial camera, Lambert target, heat flux sensor, cooling system, and a data acquisition and processing system. The size of the Lambert target is 1800 mm×400 mm, and the surface is sprayed with Al_2O_3 with a purity of 99%. Additionally, its diffuse reflectance is 95%, and the working temperature is greater than 1000°C. After the test, it can be lowered to the initial position through the pulley device. The camera is installed at the center line intersection of the Lambert target and mirror field plane, and the lens points to the Lambert target. To prevent the strong lights reflected from the surface of the Lambert target from saturating the CCD array, a neutral density attenuation filter is placed in front of the lens. The parameters of the CCD camera are shown in Table 1. The heat flux sensors are thermopile sensors, and the energy flux is converted by means of test voltage. The sensor response value is 1.55 kW/(m^2·MV), the test voltage range is 0–12.903 MV, and the resolution is 0.001 55 kW/m^2, which is calculated according to the heat flux calibration curve provided by the manufacturer. The coolant circulation will be used for cooling to prevent the high surface temperature of the heat flux sensor from affecting the test accuracy. The data acquisition and processing system will analyze and process the output values of the heat flux sensor and CCD camera.

Table 1 Parameters of the CCD camera

Model	BT-23C1214MP5
Resolution ratio	5 m
Focal distance	12 mm
Field angle	46.6°×39°×30.3°
CPC Height from mirror/mm	3000
Adjustment range	∞
Image plane size/inches	2/3
Overall dimension/mm	Φ32.9 × 40.5

3.2 Test principle

Because the lights are not focused, the average GV_{mean} of gray data GV_i for each pixel on the Lambert target is

called the average dark output [39], which can be calculated with Eq. (6):

$$GV_{\text{mean}} = \frac{1}{N_{\text{total}}} \sum_{\text{i=1}}^{N_{\text{total}}} GV_{\text{i}} \tag{6}$$

where N_{total} is the total pixel number of the measurement system. Due to the Lambertian property of the Lambertian target surface, the brightness distribution of the target surface and the energy flux distribution are linear because it is viewed from all directions. The gray value of the picture taken by the CCD camera is also linear with the brightness distribution of the target surface. Therefore, the following relationship equation can be obtained:

$$E = F_{\text{c}} \cdot GV \tag{7}$$

where E is the measured value of energy flux; F_{c} is the scale coefficient; and GV is the gray value output from the CCD image, which can be extracted by a MATLAB program. If the scale coefficient F_{c} can be obtained, the gray value of each pixel in the CCD camera can be converted into the energy flux value at the corresponding position. The test system uses two heat flow sensors to test the energy flux values at different positions on the Lambert target surface. Finally, the proportional coefficient F_{c} between the two can be obtained according to the test energy flux value and the gray value. Then, the energy flux values at each position on the target surface can be obtained.

$$E_i = E_0 + \frac{|E_1 - E_0|}{|GV_1 - GV_0|} \times (GV_i - GV_0) \tag{8}$$

where E_0 is the indication of energy flow sensor 1; E_1 is the indication of energy flow sensor 2; GV_0 is the gray value at the installation of energy flow sensor 1; GV_1 is the gray value at the installation of energy flow sensor 2; E_i is the energy flux at point i of the Lambert target; and GV_i is the gray value at point i of Lambert target.

3.3 Uncertainty analysis

The uncertainty factors affecting the measurement results of the energy flux mainly include the repeatability of energy flux measurement, the accuracy of heat flow sensor, the accuracy of the CCD camera, and the non-Lambertian characteristics of the Lambert target. Moreover, each uncertainty component is independent of one another. As for each component, the root value for the square sum of relative standard uncertainty is used to synthesize the relative standard uncertainty of E.

$$u_c = \sqrt{u_1^2 + u_2^2 + u_3^2 + u_4^2} \tag{9}$$

where u_{c} is the relative standard uncertainty of the energy flux; u_1 is the uncertainty component caused by the repeatability of measurement; u_2 is the uncertainty component caused by the heat flux sensor; u_3 is the uncertainty component caused by the accuracy of CCD camera; and u_4 is the uncertainty component caused by the error of Lambert target.

During the period where there is no cloud cover or irradiance, the ambient wind speed and the ambient temperature are stable, and the energy flux distribution of the focal plane is continuously measured seven times. The average energy flux of the focal plane is also obtained, as shown in Table 2. The class A evaluation method is used to calculate the average value of E_i, kW/m^2; the standard uncertainty of measurement result u_{b1} =0.04846 kW/m^2; and the relative uncertainty u_1 = 2.19%.

Table 2 Energy flux repeatability test results

i	1	2	3	4
E_i/kW·m^{-2}	2.1086	2.1891	2.2452	2.2569
i	5	6	7	
E_i/kW·m^{-2}	2.2123	2.2181	2.2085	

The test accuracy of the heat flow sensor is 0.001 55 kW; the expanded uncertainty is ±3%; the inclusion factor k=2; the confidence probability p=95%, and the standard measurement uncertainty of u_{b2}=2.325×10^{-5} kW/m^2. The class B evaluation method is also selected, and the relative uncertainty of u_2 caused by the test accuracy of the energy flow sensor is 1.5%. The extended uncertainty of the CCD camera is 1.25% and the resolution is 1600×1200. As for the target imaging of 1820 mm×400 mm, the physical distance L represented by a pixel is 1.1375 mm. If the class B evaluation method is adopted and the confidence factor $k = \sqrt{3}$ is taken according to the uniform distribution, then the standard uncertainty u_{b3} is 0.0082 mm and the relative uncertainty u_3 is 0.72%. The surface of the Lambert target is Al_2O_3 coating with a purity of 99%, thickness of 0.5 mm, hardness of HRC68-73, and diffuse reflectance of 95%. According to the experience, the target error u_4 caused by Lambert characteristics is ±(0.5%–2%).

The relative standard uncertainty of the energy flux test can then be calculated to be 3.44% by substituting the relative standard uncertainty of each component into Eq. (9).

3.4 Experimental method

The experimental device was located on the roof of a 4-story building in Hohhot. There were no high-rise buildings around, and there was no obvious source of pollutants. The experimental time was from March 22 to May 16, 2021. The silver-plated mirrors with the same material as Linear Fresnel reflector was selected, which was divided into samples with a size of 40 mm×25 mm× 2 mm. The sample was fixed on the surface of the mirror for a 35-day natural dust deposition experiment. The dust

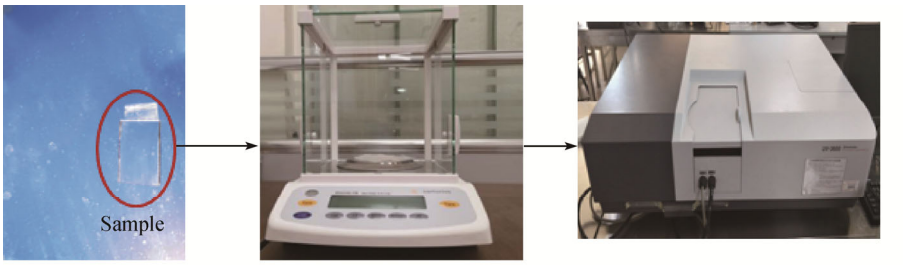

Fig. 3 Indoor experimental setup

density, cleanliness factor, and system energy flux of the mirror were simultaneously tested, with Fig. 3 showing the dust sample experimental device. The BSA2245-CW electronic balance with a measuring range of 0 to 210 g and accuracy of 0.0001 g was used to test the mass of the dust sample and clean sample. The dust mass of the mirror was then obtained. The dust density is the dust mass per unit area of sample, and the UV-3600 spectrophotometer was used to test the relative reflectivity of samples before and after dust accumulation. The result of the spectrophotometer is the relative value, and the experimental wavelength range was 185 nm to 3300 nm. The experimental process was carried out indoors. First, the clean standard sample is put into spectrophotometer. Then, the dust accumulation sample is put into spectrophotometer as the benchmark. Thus, the relative reflectivity of the sample before and after dust accumulation can be obtained.

4. Results and Discussion

4.1 Influence of mirror dust on light spot

As for the LFRC with a north-south placement and an east-west horizontal tracking of the sun, since the Sun-Earth line is not perpendicular to the Earth's axis, the solar ray is generally incident obliquely. The direct solar radiation G_b that actually irradiates on the concentrator surface can be calculated by the measured direct solar radiation intensity G_D and the cosine value of solar incidence angle θ. The direct solar radiation intensity G_D is measured by the BSRN3000 Radiation Observation system.

$$G_b=G_D\cdot\cos\theta \tag{10}$$

Fig. 4 shows the rainbow diagram of the energy flux distribution on the focal plane of the linear Fresnel system under different dust accumulation times. The figure is divided into five color representative areas: dark blue, light blue, green, yellow, and red. The corresponding energy flux values are 0 kW/m^2, 1.3750 kW/m^2, 2.7500 kW/m^2, 4.1250 kW/m^2, and 5.5000 kW/m^2, respectively. As the color trends toward red, the energy flux increases at this position. Also, Fig. 4(b)–(f) correspond to the six working conditions of the LFRC mirror cleaning of dust accumulation for 5 days, 12 days, 18 days, 28 days, and 35 days, respectively. Since direct solar radiation has impact on the energy flux, the test results of the light spot of G_b=750 W/m^2 were selected for the comparative analysis to compare the impact of dust accumulation on the light spot. The areas of red on the light spot decrease with the increase in dust accumulation days, indicating that the energy flux of the light spot decreases with the dust deposition day increasing. When the dust accumulates for 35 d, the average energy flux on the light spot decreases from 3.6748 kW/m^2 to 2.0911 kW/m^2, which is a decrease of about 43%. Furthermore, it was found that the energy flux distribution of the light spot was relatively uniform and neat in the early stages of dust accumulation on the mirror. However, the energy flux distribution of the light spot becomes uneven and the focusing energy diverges with the increase in dust accumulation time. Since the dust on the linear Fresnel reflector will absorb and scatter the incident light, and they can change the propagation paths of the lights and cause optical losses, keeping the mirror clean is important.

To quantitatively characterize the influence of dust accumulation on the light spot of the linear Fresnel system, referring to the provisions on light spot unevenness in the international standard IEC60904-9, it is introduced as the evaluation index for the energy uniformity of the light spot, which is defined as follows:

$$\Delta E=1-\frac{E_{max}-E_{ave}}{E_{max}+E_{ave}}\times 100\% \tag{11}$$

where ΔE is the uniformity of light spot; E_{max} is the maximum energy flux on the light spot; and E_{ave} is the average energy flux on the light spot. As shown in Fig. 5, the spot uniformity decreases by about 5% after the first dust accumulation on the linear Fresnel reflector. However, in the later stage, with the increase in time for dust accumulation, the spot uniformity does not decrease significantly and remains at about 68%. It indicates that the dust accumulation on the mirror will cause an uneven energy distribution on the light spot, but the spot uniformity does not change with the increase in the amount of dust. Since the dust particle has non-transparent properties, the lights incident on linear

Fresnel reflector are absorbed and scattered by the dust. Owing to the difference in the shape and size of the dust particles on the mirror, the absorption and scattering of lights by the dust are also different, leading to an uneven energy distribution on the light spot after the dust accumulation on the mirror.

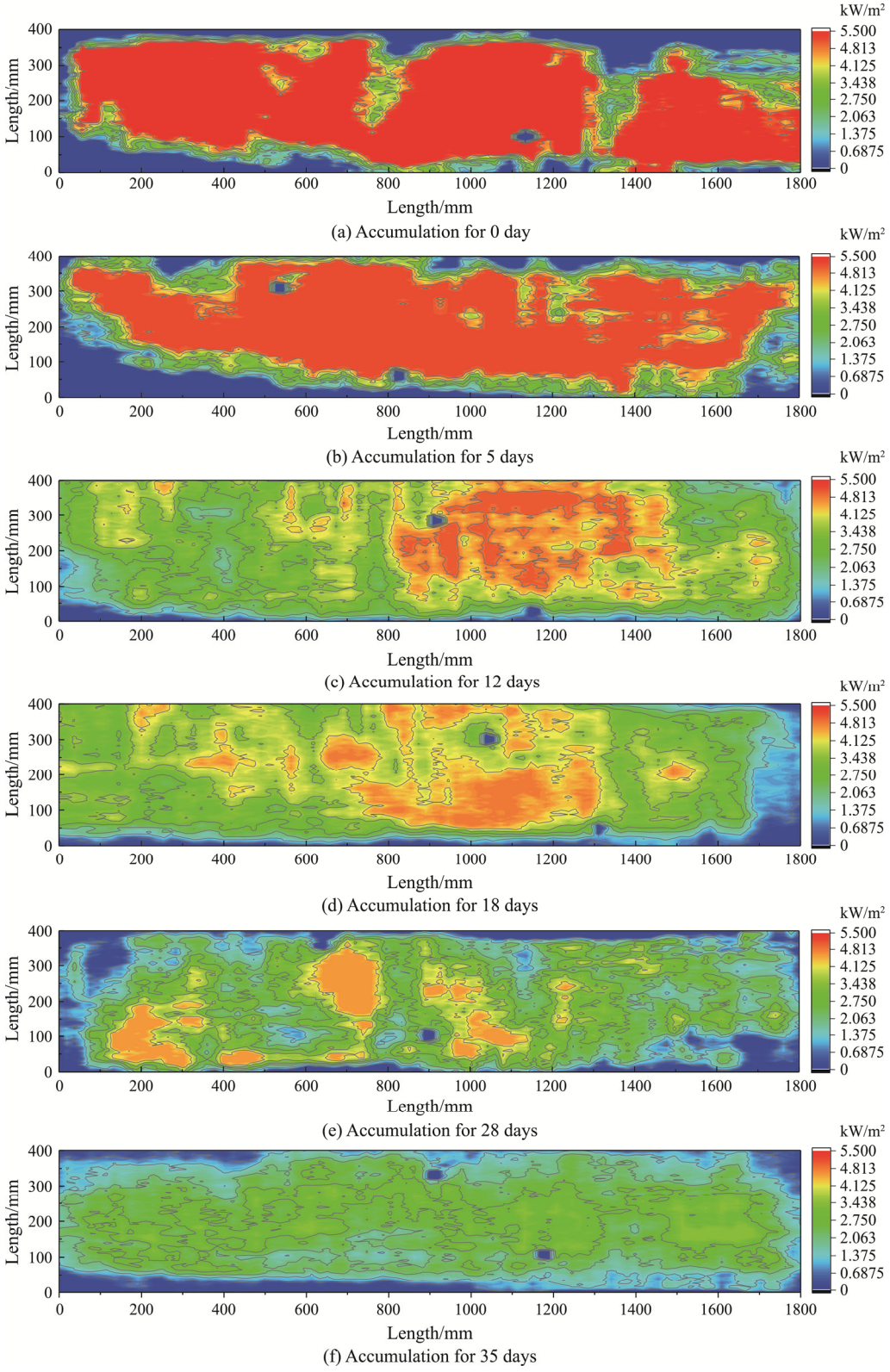

Fig. 4 Energy flux distribution on the Lambert target

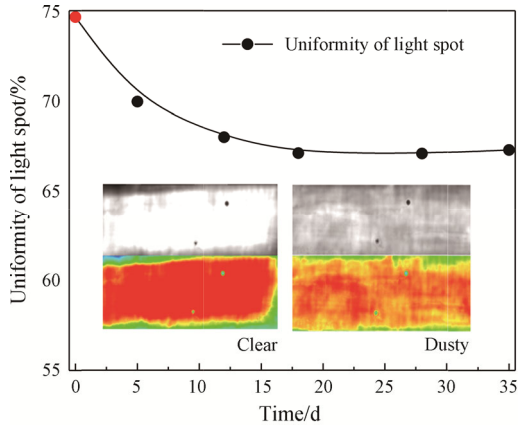

Fig. 5 Uniformity of light spot

4.2 Energy flux distribution of the system under different dust accumulation times

The D_b value is about 700 W/m^2, and the experimental data at the same position of the Lambert target under various working conditions are taken as the average value. Fig. 6(a) and (b) show the variation of the average values of energy flux in the length direction and the width direction of the Lambert target under different dust accumulation times, respectively. As shown in Fig. 6(a), the energy flux along the length of the Lambert target presents a wave trend, which indicates that the energy distribution on the receiver is uneven and the average energy flux decreases with the increase in dust accumulation time. When the dust accumulated for 35 d, the average energy flux on the receiver was about 1.4986 kW/m^2 lower than that in the clean state, with a decrease in range of approximately 48%. Similarly, as shown in Fig. 6(b), with the increase in dust accumulation time, the energy flux also presented a downward trend. When the dust accumulated for 35 d, the energy flux decreased by an average of 1.5894 kW/m^2. The average energy flux in the width direction of the Lambert target first increased and then decreased. The variation of the energy flux in a certain width range in the middle is relatively stable. If this range is defined as a "focusing light band", it can be found that the dust accumulation on mirror is wider than the "focusing light band" corresponding to the clean mirror. Since the scattering and absorption of light caused by the dust accumulation disperse the energy of the focal plane, the "focused light band" after dust accumulation in the mirror area is wider.

Fig. 7 reflects the variation of dust density and energy flux peak and mean with the dust accumulation time. The dust density increases with the increase in dust accumulation time. After undergoing dust accumulation for 35 d, the dust density reached 4.33 g/m^2. In the first 28 d of dust accumulation, the dust density increased by an average of 0.08 g/m^2 per day. There was a dust storm during the dust accumulation from the 28th d to the

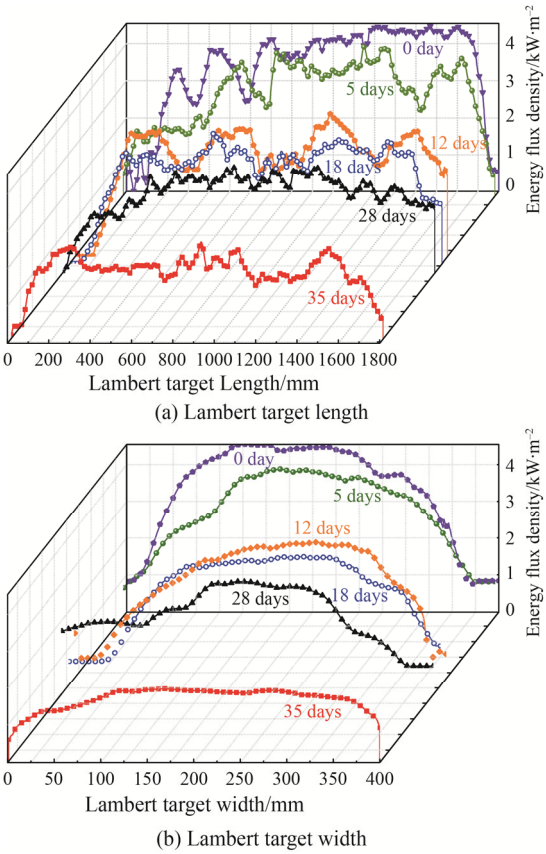

Fig. 6 Energy flux distribution of the Lambert target

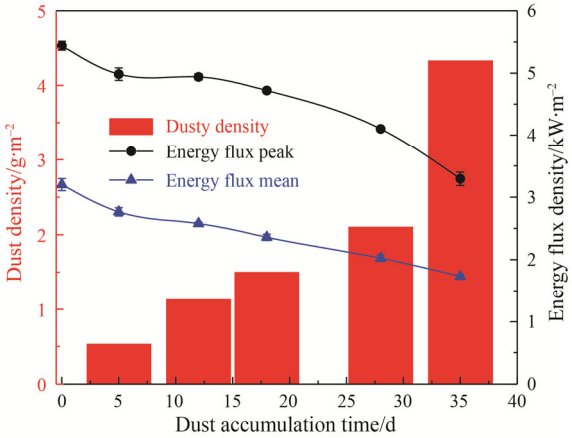

Fig. 7 Influence of reflectance on energy flux

35th d period, so the dust density on the mirror increased rapidly during this period. The energy flux was reduced with the dust density increased. When the dust density increased to 4.33 g/m^2, the energy flux peak decreased from 5.4412 kW/m^2 to 3.2908 kW/m^2, with a decrease of 39%. Furthermore, the energy flux mean decreased from 3.2022 kW/m^2 to 1.7814 kW/m^2 with a decrease of 47%. The increase in dust density decreased the energy flux mean more seriously than that of the energy flux peak. The dust blocked the solar radiation incident on the linear

Fresnel reflector, resulting in the reduction of reflected energy after the dust accumulated on mirror and the overall decrease in energy flux on receiver. The dust also had a certain scattering effect on the incident solar light, and these scattered lights could potentially irradiate the surface of the mirror and form refraction and reflection again. However, some lights will eventually reach the receiver. The dust particles with different shapes and sizes had different effects on the passage of the optical paths, leading to a higher energy flux in one area compared to others. Therefore, the decrease in the energy flux peak on the receiver was less than that of the energy flux mean.

Fig. 8 shows the comprehensive influence of the dust density and direct solar radiation on the average energy flux on the receiver. It can be observed that the energy flux gradually decreases with the decrease in direct solar radiation. Under the same direct solar radiation, the average energy flux on the receiver decreases as the dust density increases. As for D_b=750 W/m^2, when the dust density increases to 4.33 g/m^2, the energy flux mean of the receiver decreases by 1.5595 kW/m^2. For every 1 g/m^2 increase in the dust density, the peak energy flux of the receiver decreases by 0.3602 kW/m^2. As for D_b=650 W/m^2, the average energy flux on the receiver decreases by 0.3130 kW/m^2 for every 1 g/m^2 increase in the dust density on the mirror. As for D_b=550 W/m^2, the peak energy flux decreases by about 0.2470 kW/m^2 for every 1 g/m^2 increase in the dust density on the mirror. It is shown that the higher D_b, the greater the decrease in the average energy flux of the receiver caused by the mirror dust.

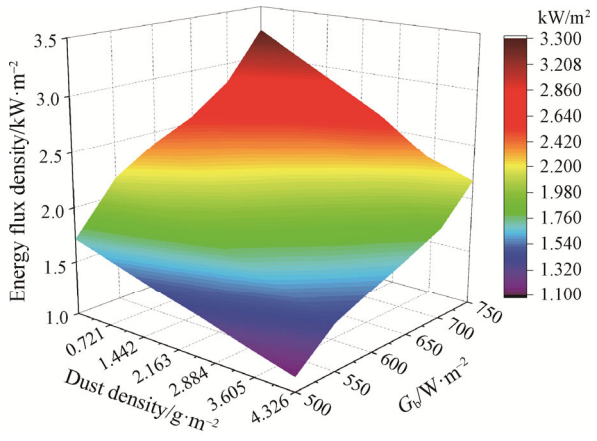

Fig. 8 Influence of dust density and G_b on the energy flux

4.3 Influence and prediction of the cleanliness of mirror factor on the optical efficiency of the system

4.3.1 Cleanliness factor and intercept factor

Fig. 9 shows the variation trend of the cleanliness factor of the mirror with wavelengths under different dust densities. The cleanliness factor increases with the increase in wavelength and decreases with the increase in dust density. The cleanliness factor decreases to 84% when the dust density reaches 4.33 g/m^2. In addition, it can be found that the impact of mirror dust on the cleanliness factor tends to decrease with the continuous increase in wavelength. For example, when the dust density is 4.33 g/m^2, the cleanliness factor in the wavelength range of 260 nm to 1000 nm decreases by 22.7%, while the cleanliness factor in the wavelength range of 1000 nm to 2600 nm decreases by just 11.4%. Moreover, the wavelength range of 380 nm to 1000 nm is the main concentrated part of solar radiation energy. Therefore, the reduction in the cleanliness factor for the mirror caused by dust accumulation cannot be ignored.

As shown in Fig. 9(b), to explore the variation law of the cleanliness factor, data fitting is carried out for the average value of the cleanliness factor under different dust densities. In addition, the mathematical relationship between the cleanliness factor and the dust density is obtained, as shown in Eq. (12):

$$\zeta=99.206\ 48-4.4266\delta+0.265\delta^2 \tag{12}$$

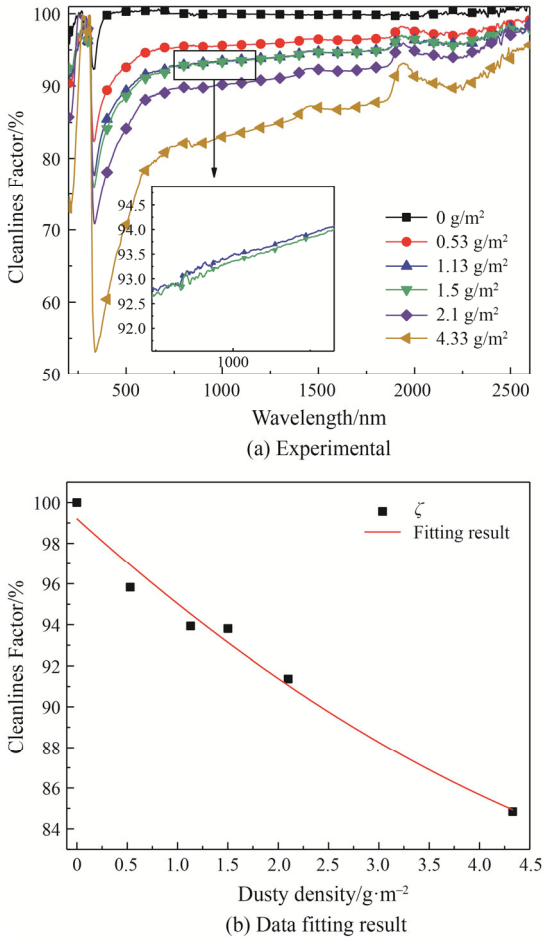

Fig. 9 Effect of dust density on the cleanliness factor

where δ represents the dust density on the mirror (g/m^2) and ζ represents the cleanliness factor of mirror. The goodness-of-fit regression equation is 0.97 and the square sum of the residual is 2.73, which can better reflect the variation law of the cleanliness factor with the dust density of the mirror.

Fig. 10 shows the variation of the focal plane energy and collection factor under different dust accumulation densities. It can be observed that the collection factor and the focal plane energy decrease with the increase in mirror dust density. With the increase in direct solar radiation, the focal plane energy also increases gradually, though the collection factor essentially does not change with the increase of direct solar radiation. As can be seen in Fig. 10(a), as the direct solar radiation increases from 500 W/m^2 to 750 W/m^2, the energy which can be received on the receiver increases from 1601.7 W to 2358.9 W for the clean mirror, and the corresponding intercept factor fluctuates at around 0.58. As for the system with a dust density of 4.33 g/m^2, the energy received on the receiver increases from 873.6 W to 1285.2 W, and the corresponding intercept factor fluctuates at about 0.31. The intercept factor of the dusty mirror decreases by about 46% compared with the clean mirror. Here, the focusing loss of the system is more serious. The above results show that the focal plane energy is affected by the direct solar radiation and the optical loss of the system, and the intercept factor is related to the optical loss of the system.

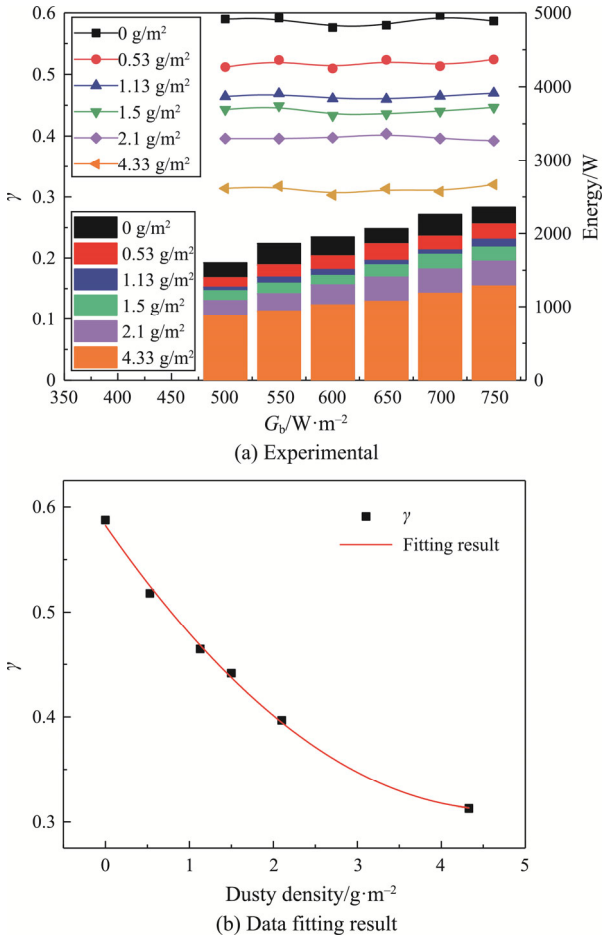

Fig. 10 Intercept factor with various dust density

As shown in Fig. 10(b), to explore the law of intercept factor with the dust density, the mathematical relationship between the intercept factor and dust density is obtained by means of data fitting according to the energy flux density experimental results, as shown in Eq. (13):

$$\gamma=0.5825-0.115\delta+0.0122\delta^2 \quad (13)$$

where δ represents the dust density (g/m^2) and γ represents the intercept factor. The goodness-of-fit regression equation is 0.99 and the square sum of the residual is 1.1095, which can better reflect the law of intercept factor with the dust density.

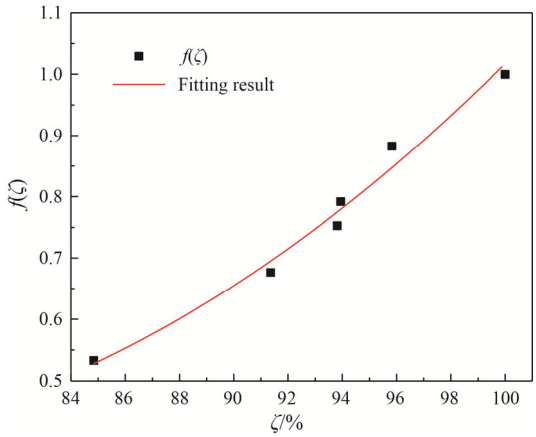

Fig. 11 Change of intercept factor correction coefficient

Fig. 11 shows the relationship between the correction coefficient of intercept factor and the cleanliness factor of mirror. As shown in Fig. 11, the correction coefficient of intercept factor increases with the increase in the cleanliness factor of mirror. When the mirror cleanliness factor is 84.84%, the correction factor of the collection factor is 0.5328. At this time, there is a large amount of energy losses caused by the dust accumulation on mirror. As the mirror cleanliness factor rises to 100%, the correction coefficient of the intercept factor is 1. In practical engineering applications, the problem of dust accumulation on mirror is inevitable. As for dedusting, it is necessary to comprehensively consider the relationship between the cleanliness factor of the mirror and the correction coefficient of the intercept factor.

$$f(\zeta)=4.2839-0.1092\zeta+7.6567\times10^{-4}\zeta^2 \quad (14)$$

where ζ represents the cleanliness factor of the mirror and $f(\zeta)$ represents the correction coefficient of the intercept factor. The goodness-of-fit regression equation is 0.98 and the square sum residual is 0.0024.

4.3.2 Optical efficiency

The optical efficiency is defined as the ratio of the energy absorbed by the receiver to the energy incident on the collector's aperture:

$$\eta_0=\frac{Q_r}{G_D A} \tag{15}$$

where η_0 represents the optical efficiency; Q_r represents the energy absorbed by the receiver, W; G_D represents the direct solar radiation projected to the concentrator, W/m^2; and A represents the area of the concentrator, m^2.

There are two types of losses in the focusing process when the solar radiation is projected to the concentrator. One is reflection loss, transmission loss, and absorption loss, while the other is focusing loss. The degree of reflection of the incident lights by the concentrator is generally characterized by the reflectivity ρ, the degree of transmission of the lights passing through the receiver glass is generally characterized by the transmittance τ, and the degree of absorption of the receiver to solar radiation is generally characterized by the absorbance α. The focusing losses of the system can be characterized by the intercept factor. The optical efficiency of concentrating collectors can be expressed as follows [40]:

$$\eta_0=\tau\alpha\rho\gamma \tag{16}$$

Linear Fresnel reflectors generally use one-axis tracking, and there will be shadows and occlusions between adjacent reflectors. The focusing losses of the LFRC also include shadow and occlusion loss, cosine loss, end loss, and geometric optical loss of the CPC. In addition, the dust accumulation on the mirror can also cause focusing loss in the LFRC, which can be characterized by the correction coefficient of the intercept factor in Eq. (14). Therefore, the optical efficiency of the LFRC can be expressed as follows:

$$\eta_0=\tau\alpha\rho\gamma\eta_{cpc}f(e)f(i)f(\zeta)\cos\theta \tag{17}$$

where η_0 represents the optical efficiency; τ represents the glass tube transmittance of collector, τ=96%; α represents the metal tube absorptivity of collector, α=96%; ρ represents the reflectivity of the mirror, ρ=97%; γ represents the intercept factor of an ideal orientation system, γ=59.47; η_{cpc} represents the geometric optical efficiency of CPC, η_{cpc}=0.9937; $f(e)$ represents the end loss coefficient of the LFRC; $f(i)$ represents the shadow and occlusion loss coefficient of the LFRC; $f(\zeta)$ represents the correction coefficient of the intercept factor; and θ represents the incident angle of light. Then, the influence of dust on the optical efficiency of the LFRC can be expressed as follows:

$$\eta_0=52.83\%\times f(e)f(i)f(\zeta)\cos\theta \tag{18}$$

The four representative days of the spring equinox, summer solstice, autumn equinox, and winter solstice are selected for optical efficiency calculation and analysis. Fig. 12 presents the variation trend of the optical efficiency with the cleanliness factor of mirror in different seasons. The optical efficiency of the LFRC in different seasons presents an increasing trend with an improvement in the cleanliness factor of mirror. When the cleanliness factor of mirror is 84.84%, the optical efficiency on the spring equinox and autumn equinox is 23.8%. The optical efficiency on the summer solstice is 27.7% and the optical efficiency on the winter solstice is just 15.8%. As the cleanliness factor of mirror reaches 100%, the optical efficiency on the spring equinox and autumn equinox can be increased by 20.9%. Also, the optical efficiency during the summer solstice can be increased by 24.4%, and the optical efficiency during the winter solstice can be increased by 13.9%. Since the light incident angle of Hohhot in the winter is larger than that in the summer, it results in a relatively high cosine loss and end loss in winter. When the cleanliness factor of mirror is the same, the optical efficiency during the summer solstice is the highest; the optical efficiency during the winter solstice is the lowest, and the optical efficiency during the spring and autumn equinoxes is almost the same. If it is supposed to ensure that the optical efficiency of the LFRC is higher than 30%, the cleanliness factor of mirror should be kept above 87% in the summer. Therefore, the mirror needs to be cleaned once every 35 days where rainfall is absent. In the spring and autumn, the cleanliness factor of mirror should be kept above 90.5%. In the absence of rainfall, the mirror needs to be cleaned once every 26 days. In winter, the mirror should be cleaned every day.

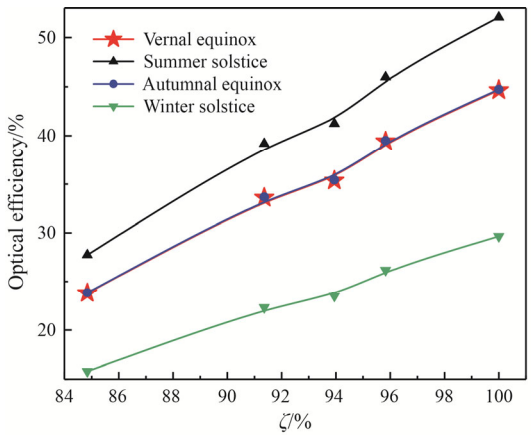

Fig. 12 Optical efficiency for various seasons

5. Conclusions

Aiming at the problem of decreasing optical efficiency of the LFRC due to dust accumulating on the mirror, an energy flux measurement device was designed and the dust accumulation test of the LFRC was carried out. The

dust density, relative reflectivity, and the energy flux under different dust accumulation times were tested. Also, the light spot distribution of LFRC was obtained. The variation of specular reflectivity caused by dust accumulation was taken as the quantitative index, and the energy obtained on the receiver was selected as the direct embodiment of focusing characteristics. Moreover, the influence of dust accumulation on the optical efficiency of the LFRC was further analyzed, and the preliminary dust removal frequency suggestions have been given for different seasons in Hohhot. The main conclusions can be summarized as follows:

(1) The dust density on the mirror gradually increases with the increase in dust accumulation time. After dust accumulation for 35 days, the dust density reached 4.33 g/m^2. On average, the dust density increased by about 0.08 g/m^2 per day.

(2) Under the same direct solar radiation, the energy flux decreased with the increase in dust accumulation time. After dust accumulation for 35 days, the energy flux peak and average decreased by 39% and 47%, respectively. After dust accumulation on mirror, the uniformity of light spot decreased by about 5%.

(3) As the dust density increases, the cleanliness factor of the mirror decreases. For every 1 g/m^2 increase in dust density, the cleanliness factor of the mirror decreased by 3.7%, and the intercept factor of the system decreased by 0.0635.

(4) With the improvement of the cleanliness factor of mirror, the optical efficiency of the LFRC gradually increased. When the cleanliness factor of mirror is the same, the optical efficiency of each season is different, which is the highest in summer and the lowest in winter, and almost the same in spring and autumn. If the optical efficiency of the system is to be greater than 30%, the mirror needs to be cleaned once every 35 days in the summer without rainfall, whereas the mirror needs to be cleaned every 26 days in spring and autumn and every day in winter.

This study can provide some guidance for the dust removal time and frequency of the linear Fresnel mirror for Hohhot in each quarter. However, since there was no rainfall during this test, and the dust composition, particle size, and transparency were different in the various regions, it is necessary to carry out further research on the physical and chemical properties of dust, as well as the impact of rainfall on dust accumulation.

Acknowledgments

The authors appreciate the financial support provided by the National Natural Science Foundation of China (No. 51766012), the Scientific Research Project of Colleges and Universities in Inner Mongolia Autonomous Region (No. NJZY21322), Major science and Technology Project of Inner Mongolia (No. 2019ZD014 and No. 2021ZD0030), the Natural Science Foundation of Inner Mongolia (No. 2019MS05025), and the Scientific Research Project of Inner Mongolia University of Technology (No. ZZ202019).

References

[1] Maisanam A.K.S., Biswas A., Sharma K.K., Integrated socio-environmental and techno-economic factors for designing and sizing of a sustainable hybrid renewable energy system. Energy Conversion and Management, 2021, 247: 114709.

[2] Liu L., Wang Z., Wang Y., Wang J., Chang R., et al., Optimizing wind/solar combinations at finer scales to mitigate renewable energy variability in China. Renewable and Sustainable Energy Reviews, 2020, 132: 110151.

[3] Zhu T., Li Q., Xuan Y., Liu D., Hong H., Performance investigation of a hybrid photovoltaics and mid-temperature methanol thermochemistry system. Applied Energy, 2019, 256: 113908.

[4] Liang H., Wang F., Yang L., Cheng Z., Shuai Y., et al., Progress in full spectrum solar energy utilization by spectral beam splitting hybrid PV/T system. Renewable and Sustainable Energy Reviews, 2021, 141: 110785.

[5] Huaxu L., Fuqiang W., Dong Z., Ziming C., et al., Experimental investigation of cost-effective ZnO nanofluid based spectral splitting CPV/T system. Energy, 2020, 194: 116913.

[6] Feng C., Shao C., Wang X., CSP clustering in unit commitment for power system production cost modeling. Renewable Energy, 2021, 168: 1217–1228.

[7] Wang Q., Huang J., Shen Z., Yao Y., Pei G., et al., Negative thermal-flux phenomenon and regional solar absorbing coating improvement strategy for the next-generation solar power tower. Energy Conversion and Management, 2021, 247: 114756.

[8] He Y., Qiu Y., Wang K., Yuan F., Wang W., et al., Perspective of concentrating solar power. Energy, 2020, 198: 117373.

[9] Abbas R., Montes M.J., Piera M., Martínez-Val J.M., Solar radiation concentration features in Linear Fresnel Reflector arrays. Energy Conversion and Management, 2012, 54: 133–144.

[10] Zhao N., Yan S., Ma X., Wu Z., Ming T., et al., Analysis of the light concentration loss of a Fresnel CPV/T System after dust accumulation. Journal of Thermal Sciences, 2021. DOI: 10.1007/s11630-021-1466-8.

[11] Yan S., Zhao S., Ma X., Ming T., Wu Z., et al., Thermoelectric and exergy output performance of a Fresnel-based HCPV/T at different dust densities.

Renewable Energy, 2020, 159: 801–811.
[12] Bouaddi S., Ihlal A., Fernández-García A., Comparative analysis of soiling of CSP mirror materials in arid zones. Renewable Energy, 2017, 101: 437–449.
[13] Azouzoute A., Merrouni A.A., Garoum M., Bennouna E.G., Richter C., Comparison of soiling effect of two different solar mirrors in mid-south of Morocco. AIP conference proceedings, 2019. DOI: 10.1063/1.5117699
[14] Elminir H.K., Ghitas A.E., Hamid R.H., El-Hussainy F., Beheary M.M., et al., Effect of dust on the transparent cover of solar collectors. Energy Conversion and Management, 2006, 47: 3192–3203.
[15] Picotti G., Borghesani P., Cholette M.E., Manzolini G., Soiling of solar collectors – Modelling approaches for airborne dust and its interactions with surfaces. Renewable and Sustainable Energy Reviews, 2018, 81: 2343–2357.
[16] Merrouni A.A., Mezrhab A., Ghennioui A., Naimi Z., Measurement, comparison and monitoring of solar mirror's specular reflectivity using two different Reflectometers. Energy Procedia, 2017, 119: 433–445.
[17] Gholami A., Saboonchi A., Alemrajabi A.A., Experimental study of factors affecting dust accumulation and their effects on the transmission coefficient of glass for solar applications. Renewable Energy, 2017, 112: 466–473.
[18] Bellmann P., Wolfertstetter F., Conceição R., Silva H.G., Comparative modeling of optical soiling losses for CSP and PV energy systems. Solar Energy, 2020, 197: 229–237.
[19] Wu Z., Yan S., Wang Z., Ming T., Zhao X., et al., The effect of dust accumulation on the cleanliness factor of a parabolic trough solar concentrator. Renewable Energy, 2020, 152: 529–539.
[20] Heimsath A., Lindner P., Klimm E., Schmid T., Moreno K.O., et al., Specular reflectance of soiled glass mirrors – Study on the impact of incidence angles. AIP conference proceedings 2016, 1734: 130009. DOI: 10.1063/1.4949219.
[21] Zhao W., Lv Y., Zhou Q., Yan W., Investigation on particle deposition criterion and dust accumulation impact on solar PV module performance. Energy, 2021, 233: 121240.
[22] Skouri S., Bouadila S., Ben Salah M., Ben Nasrallah S., Comparative study of different means of concentrated solar flux measurement of solar parabolic dish. Energy Conversion and Management, 2013, 76: 1043–1052.
[23] Ballestrin J., A non-water-cooled heat flux measurement system under concentrated solar radiation conditions. Solar Energy, 2002, 73: 159–168.
[24] Röger M., Herrmann P., Ulmer S., et al., Techniques to measure solar flux density distribution on large-scale receivers. Journal of Solar Energy Engineering, 2014, 136(3): 031013.
[25] Roldán M.I., Monterreal R., Heat flux and temperature prediction on a volumetric receiver installed in a solar furnace. Applied Energy, 2014, 120: 65–74.
[26] Xiao G., Guo K., Xu W., Ni M., Luo Z., et al., An improved method of Lambertian CCD-camera radiation flux measurement based on SMARTS (simple model of the atmospheric radiative transfer of sunshine) to reduce spectral errors. Energy, 2014, 67: 74–80.
[27] Pozzobon V., Salvador S., High heat flux mapping using infrared images processed by inverse methods: An application to solar concentrating systems. Solar Energy, 2015, 117: 29–35.
[28] Lee H., Chai K., Kim J., Lee S., Yoon H., et al., Optical performance evaluation of a solar furnace by measuring the highly concentrated solar flux. Energy, 2014, 66: 63–69.
[29] Zarei T., Abdolzadeh M., Soltani M., Aghanajafi C., Computational investigation of dust settlement effect on power generation of three solar tracking photovoltaic modules using a modified angular losses coefficient. Solar Energy, 2021, 222: 269–289.
[30] Li X., Qin H., Zhang Y., Yao W., Li Y., et al., Dust effect on the optical-thermal properties of absorber plate in a transpired solar air collector. Energy Conversion and Management, 2018, 169: 13–21.
[31] Lu J., Hajimirza S., Optimizing sun-tracking angle for higher irradiance collection of PV panels using a particle-based dust accumulation model with gravity effect. Solar Energy, 2017, 158: 71–82.
[32] Oh S., Analytic and Monte-Carlo studies of the effect of dust accumulation on photovoltaics. Solar Energy, 2019, 188: 1243–1247.
[33] Li X., Niu K., Effectively predict the solar radiation transmittance of dusty photovoltaic panels through Lambert-Beer law. Renewable Energy, 2018, 123: 634–638.
[34] Picotti G., Moretti L., Cholette M.E., Binotti M., Simonetti R., et al., Optimization of cleaning strategies for heliostat fields in solar tower plants. Solar Energy, 2020, 204: 501–514.
[35] Bouaddi S., Ihlal A., Fernández-García A., Soiled CSP solar reflectors modeling using dynamic linear models. Solar Energy, 2015, 122: 847–863.
[36] Heimsath A., Nitz P., The effect of soiling on the reflectance of solar reflector materials - Model for prediction of incidence angle dependent reflectance and attenuation due to dust deposition. Solar Energy Materials and Solar Cells, 2019, 195: 258–268.
[37] Wu Z., Yan S., Ming T., Zhao X., Zhang N., Analysis and modeling of dust accumulation-composed spherical and

cubic particles on PV module relative transmittance. Sustainable Energy Technologies and Assessments, 2021, 44: 101015.

[38] Zhao X., Chen Z., Yan S., Ming T., Wu Z., et al., Influence of dust accumulation on the solar reflectivity of a linear Fresnel reflector. Journal of Thermal Sciences, 2021, 30(5): 1526–1540.

[39] Ulmer S., Reinalter W., Heller P., et al., Beam characterization and improvement with a flux mapping system for dish concentrators. Journal of Solar Energy Engineering, 2002, 124(5): 182–188.

[40] Kalogirou S.A., Solar thermal collectors and applications. Progress in Energy and Combustion Science, 2004, 30: 231–295.